

Conical diffraction complexified: dichroism and the transition to double refraction

M V Berry and M R Jeffrey

H H Wills Physics Laboratory, Tyndall Avenue, Bristol BS8 1TL, UK

Received 22 August 2006, accepted for publication 5 October 2006

Published 1 November 2006

Online at stacks.iop.org/JOptA/8/1043

Abstract

With dichroism (anisotropic absorption), the dielectric tensor of a crystal becomes non-Hermitian, and each optic axis (diabolical point) splits into two singular axes (branch-point degeneracies). For a Gaussian beam incident on a dichroic crystal in a direction near the singular axes, the polarized light beyond the crystal is given by the same diffraction integrals as for a transparent crystal illuminated along the optic axis, but with the variables complexified. Unexpectedly, the effects of absorption and beam direction can be described with a single parameter. The theory predicts several new types of interference, visible in logarithmic intensity plots: between the nonorthogonally polarized geometrical rays, and between these rays and waves diffracted by the singular axes. The phenomena are analysed in terms of saddle-point, end-point and uniform asymptotics of the diffraction integrals.

Keywords: polarization, birefringence, non-Hermitian, crystal optics

1. Introduction

Our main purpose here is to incorporate dichroism (anisotropic absorption) into the theory of conical diffraction [1, 2], that is, conical refraction and the associated wave effects. This will extend the physical theory of conical diffraction that was begun by Hamilton in 1832 [3, 4]. Interest in the phenomenon has revived, partly as a result of the bicentenary in 2005 of Hamilton's birth, and there have been several recent developments. These include: definitive formulation of the theory for transparent biaxial crystals, greatly simplified by the realistic assumption of paraxiality [1, 5]; understanding the phenomena implied by the theory [6–8]; experimental demonstration of the theoretical predictions [9]; extension of the theory to include chirality (optical activity) [10, 11]; and extension of the theory to include nonlinearity [12].

Conical refraction is associated with degeneracy of the matrix generating the wave surface [13] (polar plot of the two refractive indices as a function of directions of plane waves). For transparent biaxial non-chiral crystals, this matrix is real symmetric, and its degeneracies take the form of conical intersections—'diabolical points' [1]—corresponding to the optic axes. Conical refraction is the physical manifestation of this degeneracy: a narrow beam directed along an optic axis

splits into a hollow cone inside the crystal, and refracts into a hollow cylinder beyond [13, 14].

With absorption (but without chirality [10]), the matrix is complex symmetric, that is, non-Hermitian. This changes the degeneracy structure radically [15]: each conical intersection splits into two branch-points, which in optics are called the singular axes [14, 16–20]. We will study beam propagation associated with these singular axes. The effect of dichroism will be quantified (section 2) by a 2-vector parameter δ .

The splitting of axes raises a problem concerning the direction of the incident beam. Should this be aimed at one of the singular axes? If so, which? Or half-way between the axes? To resolve this difficulty, we allow variation of the beam direction, specified by a second 2-vector parameter κ_0 , representing the transverse wavevector. Of course κ_0 could have been incorporated into the theory of ordinary conical diffraction, where [21] it describes the transition from conical to double refraction.

In the pioneering observations [22–24], the incident beam profile was restricted by a pinhole, but the theory is considerably simplified by studying conical diffraction for Gaussian incident beams, for which the diffraction detail is different [5, 8]. Moreover, Gaussian beams correspond to

current experiments with lasers [9, 25–27]. Therefore we will develop the theory for Gaussian beams.

With Gaussian beams, our study (section 2) reveals an unanticipated and remarkable fact: the effect of changing the direction κ_0 of the incident beam is exactly the same as introducing dichroism δ ; moreover, the two vector parameters δ and κ_0 can be replaced by a single scalar parameter u . The resulting theory is identical with that for ordinary conical diffraction by a transparent crystal, except that the variables in the theory are complex. The reason why double refraction in a transparent crystal can mimic the effect of absorption is connected with the fact that a Gaussian beam can be regarded as a bundle of complex rays [28].

Previous theory [1, 5] showed that conical diffraction by a transparent crystal is determined by a single parameter ρ_0 , defined as the radius of the geometrical cylinder beyond the crystal divided by the waist width of the incident beam. Therefore the complexified situation considered here, of biaxial birefringence plus absorption, depends on the two parameters ρ_0 and u . Interesting and subtle interference features in the light beyond the crystal occur in the regime $\rho_0 \gg 1$, corresponding to thick crystals. Isolating and understanding these features in detail requires several levels of asymptotic approximation to the theory (section 3).

We will display a number of simulated images and graphs of the light intensity. The intensities can exhibit exponentially large variations across the images. As a result, important interference fringes are concealed in direct plots of the intensity, and can be discerned only on logarithmic plots.

Although the effects of anisotropic absorption are dramatic, its cause—an imaginary part in the dielectric tensor—is likely to be small in practice. For completeness, we also consider (section 4) the opposite extreme, where all the anisotropy is in the dichroism, and the refractive properties of the crystal are isotropic.

For the constitutive equation of the crystal, assumed nonmagnetic and optically inactive, we choose the inverse complex dielectric tensor

$$\eta = \varepsilon_0 \mathbf{e}^{-1} = \begin{pmatrix} \eta_1 & 0 & 0 \\ 0 & \eta_2 & 0 \\ 0 & 0 & \eta_3 \end{pmatrix}. \quad (1.1)$$

The components of $\text{Re } \eta$ represent the principal refractive indices:

$$\text{Re } \eta_1 = \frac{1}{n_1^2} > \text{Re } \eta_2 = \frac{1}{n_2^2} > \text{Re } \eta_3 = \frac{1}{n_3^2}. \quad (1.2)$$

The optic axes are the propagation directions for which the 2×2 transverse part of $\text{Re } \eta$ is degenerate. The singular axes are the propagation directions for which the 2×2 transverse part of η itself is degenerate.

The components of $\text{Im } \eta$ represent the anisotropic absorption which is our main concern here. There is slight lack of generality in (1.1), which assumes that the principal axes of $\text{Re } \eta$ and $\text{Im } \eta$ coincide; this is true for orthorhombic crystals but not for crystals with lower symmetry. The assumption is not a serious restriction, because the phenomena to be described require only that the optic axes, generated by $\text{Re } \eta$, and the corresponding directions generated by $\text{Im } \eta$, are distinct, which is true in general for (1.1).

With polar coordinates θ, ϕ in direction space, one pair of singular axes is conveniently given [20] in stereographic coordinates Z by

$$Z = \tan \frac{1}{2} \theta \exp(i\phi) = \frac{\sqrt{\eta_1 - \eta_3} - \sqrt{\eta_2 - \eta_3}}{\sqrt{\eta_1 - \eta_2}}, \quad (1.3)$$

$$\text{and } Z^* = \tan \frac{1}{2} \theta \exp(-i\phi).$$

For a transparent crystal ($\text{Im } \eta = 0$), the optic axis lies in the plane $\phi = 0$, with polar angle [1]

$$\tan \theta = \sqrt{\frac{R_{12}}{R_{23}}}, \quad (1.4)$$

where

$$R_{ij} \equiv \text{Re}(\eta_i - \eta_j) = \frac{1}{n_i^2} - \frac{1}{n_j^2}. \quad (1.5)$$

Absorption splits this into two singular axes with azimuth angles $\pm\phi$, the angular splitting being

$$\begin{aligned} \Delta = 2\phi \sin \theta &= \frac{4}{1+|Z|^2} \text{Im } Z \\ &= \frac{R_{23} \text{Im } \eta_1 + R_{31} \text{Im } \eta_2 + R_{12} \text{Im } \eta_3}{R_{13} \sqrt{R_{12} R_{23}}}. \end{aligned} \quad (1.6)$$

2. Non-Hermitian paraxial theory

For later comparison with the dichroic case, it is helpful first to review conical diffraction for transparent crystals [1, 9], referring to the principal features by the names of their discoverers. In the interesting regime $\rho_0 \gg 1$, the typical image in planes beyond the crystal, when viewed under low resolution, consists of a Hamilton [4] bright ring: the geometrical image of the incident beam. Closer examination reveals that the ring is really two thin rings, separated by the Poggendorff [29] dark ring: an anti-caustic. Still-finer resolution reveals that inside the inner ring are Warnick–Arnold [6] fringes: interference between a geometrical ray and a wave diffracted by the diabolical point on the wave surface. At the centre of the rings, and getting more prominent further from the screen, is a bright Raman [24] spot, decorated with fringes: an axial caustic.

It is also convenient to recapitulate the paraxial theory [1] that explains these conical diffraction phenomena for transparent crystals. Geometrically, the light inside the crystal forms a cone of half-angle

$$A = \frac{1}{2} \arctan \left(n_2^2 \sqrt{R_{12} R_{23}} \right) \approx \frac{\sqrt{(n_2 - n_1)(n_3 - n_2)}}{n_2}. \quad (2.1)$$

Outside, the cone refracts into a cylinder of radius Al , where l is the thickness of the crystal. The parameter ρ_0 governing the field outside the crystal is this radius, measured in units of the beam waist width w :

$$\rho_0 \equiv \frac{Al}{w}. \quad (2.2)$$

Transverse position in the field, also measured in units of w , is specified by

$$\boldsymbol{\rho}' = \{\xi', \eta'\}. \quad (2.3)$$

Longitudinal position in the field is measured in units of the Fresnel length of the beam, by

$$\zeta \equiv \frac{l + (z - l)n_2}{n_2 k_0 w^2}, \quad (2.4)$$

where z is measured from the beam waist and k_0 is the vacuum wavenumber of the light; thus $\zeta = 0$ corresponds to the ‘focal image plane’ where the virtual image of the beam waist would be formed by an isotropic crystal with index n_2 .

In terms of these quantities, the two-component transverse electric \mathbf{D} vector beyond the crystal, for incident polarization \mathbf{d}_0 , is given by a superposition of plane waves with transverse wavevectors $\boldsymbol{\kappa}$, measured in units of w^{-1} :

$$\mathbf{D} = \frac{1}{2\pi} \int \int d\boldsymbol{\kappa} a(\boldsymbol{\kappa}) \exp(i\boldsymbol{\kappa} \cdot \boldsymbol{\rho}') \mathbf{U}_{\text{transparent}}(\boldsymbol{\kappa}) \mathbf{d}_0. \quad (2.5)$$

The origin $\boldsymbol{\kappa} = 0$ represents plane waves travelling along the optic axis. Directions $\boldsymbol{\kappa} \neq 0$ near the optic axis will be treated paraxially. $a(\boldsymbol{\kappa})$ is the Fourier transform of the profile of the incident beam, and $\mathbf{U}_{\text{transparent}}$ is the unitary operator

$$\mathbf{U}_{\text{transparent}}(\boldsymbol{\kappa}) = \exp\left\{-i\left(\frac{1}{2}\boldsymbol{\kappa}^2\zeta + \rho_0\boldsymbol{\kappa} \cdot \mathbf{S}\right)\right\}, \quad (2.6)$$

conveniently written in terms of the Pauli matrices

$$\mathbf{S} = \{\sigma_3, \sigma_1\} = \left\{ \begin{pmatrix} 1 & 0 \\ 0 & -1 \end{pmatrix}, \begin{pmatrix} 0 & 1 \\ 1 & 0 \end{pmatrix} \right\}. \quad (2.7)$$

As previously emphasized [9], the theory based on (2.5) describes not only the light beyond the crystal but also the virtual field within and before the crystal, which can easily be imaged onto a screen.

Dichroism can be incorporated by making the exponent in the operator in (2.6) non-Hermitian, so \mathbf{U} itself is nonunitary:

$$\boldsymbol{\kappa} \cdot \mathbf{S} \Rightarrow (\boldsymbol{\kappa} + i\boldsymbol{\delta}) \cdot \mathbf{S}. \quad (2.8)$$

In terms of the splitting Δ of the singular axes, given by (1.6),

$$|\boldsymbol{\delta}| \equiv \delta = \frac{1}{2}\Delta n_2 k_0 w. \quad (2.9)$$

In writing (2.8), we are ignoring the $\boldsymbol{\kappa}$ -dependence of $\boldsymbol{\delta}$, because we treat $\boldsymbol{\delta}$ as a (singular) perturbation; alternatively stated, we assume that the optic axes of absorption ($\text{Im } \boldsymbol{\eta}$) are distinct from those of birefringence ($\text{Re } \boldsymbol{\eta}$).

$\boldsymbol{\delta}$ is proportional to the traceless (anisotropic) part of $\text{Im } \boldsymbol{\eta}$. To guarantee that the crystal is absorbing rather than amplifying, we should add a diagonal (isotropic) part to $\text{Im } \boldsymbol{\eta}$, sufficiently large to make $\text{Tr } \text{Im } \boldsymbol{\eta} < 0$; we do not write this explicitly because its only effect on the field beyond the crystal is multiplication by a z -dependent attenuation factor. We note the fundamental difference between the nonunitary modification (2.8), describing absorption, and the modification [10] required to include chirality (not considered here), which involves keeping \mathbf{U} unitary while adding the imaginary Pauli matrix σ_2 .

With (2.8), the matrix in (2.5) becomes

$$\mathbf{U}(\boldsymbol{\kappa}) = \exp\left\{-i\left(\frac{1}{2}\boldsymbol{\kappa}^2\zeta + \rho_0(\boldsymbol{\kappa} + i\boldsymbol{\delta}) \cdot \mathbf{S}\right)\right\}. \quad (2.10)$$

The singular axes (degeneracies) occur at directions $\boldsymbol{\kappa}_d$, satisfying

$$(\boldsymbol{\kappa}_d + i\boldsymbol{\delta}) \cdot (\boldsymbol{\kappa}_d + i\boldsymbol{\delta}) = 0 \Rightarrow \boldsymbol{\kappa}_d = \pm\{-\delta_y, \delta_x\}. \quad (2.11)$$

We represent the Gaussian incident beam, in direction $\boldsymbol{\kappa}_0$, by its Fourier transform

$$a(\boldsymbol{\kappa}) = \exp\left\{-\frac{1}{2}(\boldsymbol{\kappa} - \boldsymbol{\kappa}_0)^2\right\}. \quad (2.12)$$

Thus the field at $\{\boldsymbol{\rho}', \zeta\}$ is

$$\mathbf{D} = \frac{1}{2\pi} \int \int d\boldsymbol{\kappa} \exp\{-i\mathbf{F}(\boldsymbol{\kappa})\} \mathbf{d}_0, \quad (2.13)$$

where the non-Hermitian operator in the exponent is

$$\mathbf{F}(\boldsymbol{\kappa}) = -\frac{1}{2}i(\boldsymbol{\kappa} - \boldsymbol{\kappa}_0)^2 - \boldsymbol{\kappa} \cdot \boldsymbol{\rho}' + \frac{1}{2}\boldsymbol{\kappa}^2\zeta + \rho_0(\boldsymbol{\kappa} + i\boldsymbol{\delta}) \cdot \mathbf{S}. \quad (2.14)$$

We now make several transformations, whose merit will soon become clear. It is obviously convenient to define the modified variables

$$\tilde{\boldsymbol{\kappa}} \equiv \boldsymbol{\kappa} + i\boldsymbol{\delta}, \quad \tilde{\zeta} \equiv \zeta - i. \quad (2.15)$$

We also use the less obvious parameter combination

$$\mathbf{u} \equiv \zeta\boldsymbol{\delta} - \boldsymbol{\kappa}_0 \equiv u\mathbf{e}_\xi, \quad (2.16)$$

and the transverse coordinate shift and complex scaling

$$\boldsymbol{\rho} \equiv \boldsymbol{\rho}' - \boldsymbol{\delta} = \{\xi, \eta\}, \quad \tilde{\boldsymbol{\rho}} \equiv \boldsymbol{\rho} + iu\mathbf{e}_\xi \equiv \left\{ \tilde{\rho} \cos \tilde{\phi}, \tilde{\rho} \sin \tilde{\phi} \right\} \quad (2.17)$$

where in (2.16) we have chosen the orientation of the transverse ξ axis to lie along the direction of \mathbf{u} .

After these transformations, the operator (2.14) becomes

$$\mathbf{F}(\boldsymbol{\kappa}) = \tilde{\mathbf{F}}(\tilde{\boldsymbol{\kappa}}) = \frac{1}{2}\tilde{\boldsymbol{\kappa}}^2\tilde{\zeta} - \tilde{\boldsymbol{\kappa}} \cdot \tilde{\boldsymbol{\rho}} + \rho_0\tilde{\boldsymbol{\kappa}} \cdot \mathbf{S} + F_0, \quad (2.18)$$

where

$$F_0 \equiv i\left(\boldsymbol{\delta} \cdot \boldsymbol{\rho} + \frac{1}{2}(\delta^2 - \kappa_0^2)\right) + \boldsymbol{\delta} \cdot \boldsymbol{\kappa}_0 - \frac{1}{2}\delta^2\zeta, \quad (2.19)$$

so that (after a complex shift of integration contour)

$$\mathbf{D} = \frac{1}{2\pi} \int \int d\tilde{\boldsymbol{\kappa}} \exp\{-i\tilde{\mathbf{F}}(\tilde{\boldsymbol{\kappa}})\} \mathbf{d}_0. \quad (2.20)$$

Since the operator \mathbf{U} involves only 2×2 matrices, it is easy to evaluate the exponential and perform the integration over the direction of $\tilde{\boldsymbol{\kappa}}$, giving

$$\mathbf{D} = \exp\{-iF_0\} \begin{pmatrix} B_0 + B_1 \cos \tilde{\phi} & B_1 \sin \tilde{\phi} \\ B_1 \sin \tilde{\phi} & B_0 - B_1 \cos \tilde{\phi} \end{pmatrix} \mathbf{d}_0, \quad (2.21)$$

involving the fundamental integrals

$$\begin{aligned} B_0(\tilde{\rho}, \tilde{\zeta}; \rho_0) &= \int_0^\infty d\tilde{\kappa} \tilde{\kappa} \exp\left\{-\frac{1}{2}i\tilde{\zeta}\tilde{\kappa}^2\right\} J_0(\tilde{\kappa}\tilde{\rho}) \cos(\tilde{\kappa}\rho_0) \\ B_1(\tilde{\rho}, \tilde{\zeta}; \rho_0) &= \int_0^\infty d\tilde{\kappa} \tilde{\kappa} \exp\left\{-\frac{1}{2}i\tilde{\zeta}\tilde{\kappa}^2\right\} J_1(\tilde{\kappa}\tilde{\rho}) \sin(\tilde{\kappa}\rho_0). \end{aligned} \quad (2.22)$$

The number of variables can be reduced from three to two by rescaling $\tilde{\kappa}$, but the forms (2.22) are convenient for later analysis.

The integrals (2.22) are exactly those in the theory of conical diffraction without dichroism (i.e. $\boldsymbol{\delta} = 0$), with light directed along the optic axis (i.e. $\boldsymbol{\kappa}_0 = 0$). The four new parameters (two components of each of the vectors $\boldsymbol{\delta}$ and

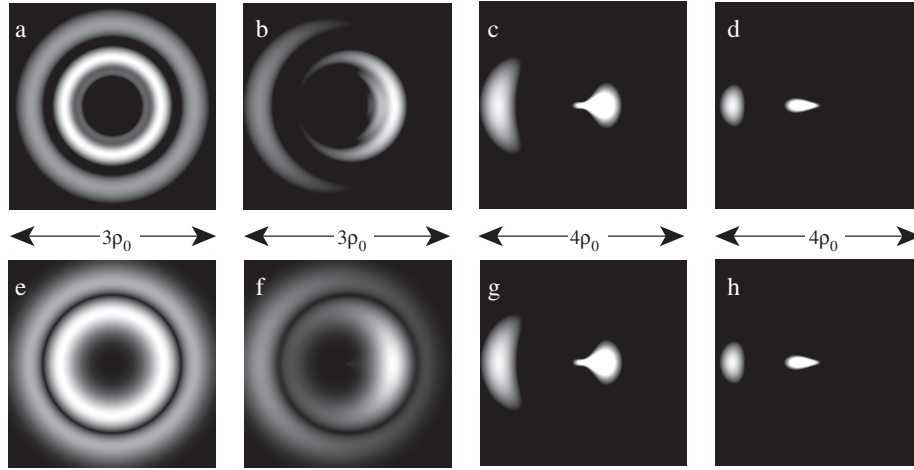


Figure 1. Density plots of exact intensity (equations (2.32) and (2.22)) in the $\rho = \{\xi, \eta\}$ plane, showing transition between conical (a) and double (c), (d) refraction, for $\rho_0 = 20$, $\zeta = 6$, and: (a) $u = 0$, (b) $u = 1/2$, (c) $u = 2$, (d) $u = 5$. In (c) and (d) the brighter (right-hand) spots are saturated, in order to display the fainter spots. (e)–(h) Corresponding plots for the geometrical optics intensity (equations (2.32) and (3.3)).

κ_0) are represented by the single parameter u . Moreover, the form of (2.16) implies the unexpected fact that for any absorption δ and any observation distance ζ , it is possible to choose a beam direction κ_0 for which u vanishes, so the conical diffraction pattern is identical, up to a prefactor, to that for a transparent crystal illuminated along the optic axis. The prefactor $\exp\{-iF_0\}$ in (2.21) simply multiplies the image intensities $|\mathbf{D}|^2$ by the exponential ramp $\exp\{2\delta \cdot \rho\}$; in the images to be presented later, we will not include this factor.

The only effect of δ and κ_0 on the diffraction integrals is to complexify the radial coordinate, whose length and direction are given (cf (2.17)) by

$$\begin{aligned} \tilde{\rho}^2 &\equiv \tilde{\rho} \cdot \tilde{\rho} = (\xi + iu)^2 + \eta^2, \\ \cos \tilde{\phi} &= \frac{\xi + iu}{\tilde{\rho}}, \quad \sin \tilde{\phi} = \frac{\eta}{\tilde{\rho}}. \end{aligned} \quad (2.23)$$

In the next section, an important role will be played by the ‘branch-points’ in the ρ plane where the complex length vanishes, namely

$$\tilde{\rho}^2 = 0 \Rightarrow \rho = \rho_{b\pm} = \{0, \pm u\}. \quad (2.24)$$

Around each of these branch-points, $\tilde{\rho}$ changes sign. Of course \mathbf{D} must be single-valued: in (2.21), B_0 (2.22) is single-valued because J_0 is an even function of $\tilde{\rho}$, and the sign change of B_1 , arising from the odd function J_1 , is compensated by sign changes in $\cos \tilde{\phi}$ and $\sin \tilde{\phi}$ (2.23).

For later interpretation in terms of geometrical optics, it is convenient to define the sum and difference integrals

$$A_+ \equiv B_0 + B_1, \quad A_- \equiv B_0 - B_1. \quad (2.25)$$

In terms of these, (2.21) becomes

$$\mathbf{D} = \frac{1}{2} \exp\{-iF_0\} (A_+ \mathbf{m}_+ + A_- \mathbf{m}_-) \cdot \mathbf{d}_0, \quad (2.26)$$

where

$$\begin{aligned} \mathbf{m}_+ &= \begin{pmatrix} 1 + \cos \tilde{\phi} & \sin \tilde{\phi} \\ \sin \tilde{\phi} & 1 - \cos \tilde{\phi} \end{pmatrix}, \\ \mathbf{m}_- &= \begin{pmatrix} 1 - \cos \tilde{\phi} & -\sin \tilde{\phi} \\ -\sin \tilde{\phi} & 1 + \cos \tilde{\phi} \end{pmatrix}. \end{aligned} \quad (2.27)$$

We note in passing that A_{\pm} are the coefficients in the expansion of the electric field in terms of the local eigenvectors of the operator (2.18):

$$\mathbf{D} = \exp\{-iF_0\} [A_+ (\mathbf{d}_+ \cdot \mathbf{d}_0) \mathbf{d}_+ + A_- (\mathbf{d}_- \cdot \mathbf{d}_0) \mathbf{d}_-], \quad (2.28)$$

where

$$\mathbf{d}_+(\tilde{\rho}) = \begin{pmatrix} \cos \frac{1}{2}\tilde{\phi} \\ \sin \frac{1}{2}\tilde{\phi} \end{pmatrix}, \quad \mathbf{d}_-(\tilde{\rho}) = \begin{pmatrix} \sin \frac{1}{2}\tilde{\phi} \\ -\cos \frac{1}{2}\tilde{\phi} \end{pmatrix}. \quad (2.29)$$

In the ρ plane, the eigenvectors are not single-valued. Because of the factors $1/2$, and the sign change of $\tilde{\rho}$, \mathbf{d}_{\pm} acquire, in a circuit of each branch-point (2.24), the phase factors $\pm i$ familiar around degeneracies (‘exceptional points’) of complex symmetric matrices [30], making them singularities of index $\pm 1/4$ [20].

It is easier to observe not \mathbf{D} itself but the light intensity I . This is

$$I = \mathbf{D}^* \cdot \mathbf{D} = \frac{1}{4} \exp\{2 \operatorname{Im} F_0\} \mathbf{d}_0^* \cdot \mathbf{M} \cdot \mathbf{d}_0, \quad (2.30)$$

where

$$\mathbf{M} = (A_+^* \mathbf{m}_+^\dagger + A_-^* \mathbf{m}_-^\dagger) (A_+ \mathbf{m}_+ + A_- \mathbf{m}_-). \quad (2.31)$$

This can be calculated without difficulty for any incident polarization \mathbf{d}_0 . For our later illustrations, however, we will consider unpolarized light, which is the average of I over any two orthogonal incident polarizations. A short calculation gives the simple result

$$\begin{aligned} \exp\{-2 \operatorname{Im} F_0\} I_{\text{unpolarized}} &= \frac{1}{8} \operatorname{Tr} \mathbf{M} \\ &= |B_0|^2 + |B_1|^2 (|\cos \tilde{\phi}|^2 + |\sin \tilde{\phi}|^2) \\ &= \frac{1}{4} [(|A_+|^2 + |A_-|^2) (1 + |\cos \tilde{\phi}|^2 + |\sin \tilde{\phi}|^2) \\ &\quad + 2 \operatorname{Re} A_+^* A_- (1 - |\cos \tilde{\phi}|^2 - |\sin \tilde{\phi}|^2)]. \end{aligned} \quad (2.32)$$

Figure 1 shows the transition between the Hamilton–Poggendorff rings (figures 1(a), (b), (e), (f)) and the deformed pair of images characteristic of double refraction (figures 1(c), (g), (d), (h)) as u increases from zero. This transition is

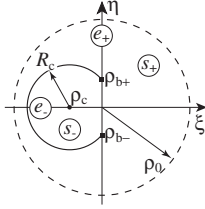


Figure 2. Schematic diagram of principal features of dichroic conical diffraction images, drawn for $\rho_0 = 20$, $u = 6$, $\zeta = 2.8$. Dashed circle: Hamilton ring, radius ρ_0 ; full circle: dark ring (3.7) where two geometrical contributions cancel, radius R_c , centre ρ_c ; square dots: branch-points (2.24) at $\rho_{b\pm}$. The regions where the contributions from the saddles s_{\pm} (geometrical rays (3.3)) and endpoints e_{\pm} (waves (3.11) and (3.15) scattered from degeneracies) dominate are also indicated.

expected for a transparent crystal, as the orientation of the incident beam deviates from the optic axis, but the same behaviour is surprising when the incident beam direction is fixed while the strength of the dichroism is increased.

An important implication of (2.32), to be explored in the next section (and not apparent in figure 1), arises from the complexification introduced by dichroism and the Gaussian beam. This makes the angle $\tilde{\phi}$ complex, so that $|\cos\tilde{\phi}|^2 + |\sin\tilde{\phi}|^2 \neq 1$ (cf (2.23)). Then the interference term $\text{Re } A_+^* A_-$ between the contributions from A_+ and A_- can give a non-zero contribution. Alternatively stated, this interference of unpolarized light is a physical consequence of the fact that the eigenvectors (2.29) of the non-Hermitian operator are nonorthogonal. Absorption can introduce similar effects for the interference of initially unpolarized plane waves in conoscopic figures [20].

3. Asymptotics

It seems that the basic integrals (2.22) cannot be expressed in closed form in terms of standard special functions. Nevertheless, the rich phenomena that emerge when $\rho_0 \gg 1$ can be understood using asymptotics. In this section we describe a series of asymptotic approximations, each capturing different aspects of the light beyond the crystal, including not only the most prominent features but several kinds of subtle interference. The different phenomena are associated with asymptotic contributions from the saddle-points and end-points of the integrals representing A_+ and A_- , relevant in different parts of the images as indicated schematically in figure 2, whose significance will emerge in the remainder of this section.

Most fundamental is geometrical optics, derived by applying the method of stationary phase to the double integral (2.13) or, more conveniently, the single integrals (2.22). We interpret ‘geometrical’ in a generalized sense, because the ‘rays’—saddle-points of the integrals over $\tilde{\kappa}$ —are complex, as a result of the complexification introduced by dichroism and the Gaussian beam. The approximation of the integrals A_{\pm} , defined in (2.25), begins by assuming that ρ is not very close to one of the branch-points (2.24), and applying the following standard large-argument forms for the Bessel functions in (2.22) [31]:

$$J_0(\tilde{\kappa}\tilde{\rho}) \cos(\tilde{\kappa}\rho_0) \pm J_1(\tilde{\kappa}\tilde{\rho}) \sin(\tilde{\kappa}\rho_0) \approx \sqrt{\frac{2}{\pi\tilde{\rho}}} \cos\left\{\tilde{\kappa}(\tilde{\rho} \mp \rho_0) - \frac{1}{4}\pi\right\}. \quad (3.1)$$

Thus

$$A_{\pm} \approx \sqrt{\frac{2}{\pi\tilde{\rho}}} \int_0^{\infty} d\tilde{\kappa} \tilde{\kappa}^{1/2} \exp\left\{-\frac{1}{2}i\tilde{\zeta}\tilde{\kappa}^2\right\} \cos\{\tilde{\kappa}(\tilde{\rho} \mp \rho_0) - \frac{1}{4}\pi\}. \quad (3.2)$$

The second step is to split the cosines into their component exponentials, and treat the resulting exponentials in the integrands as fast-varying, justifying the standard application of the method of stationary phase and leading to the simple result

$$A_{\pm} \approx A_{\pm\text{geom}} = -\frac{\mu_{\pm}}{\tilde{\zeta}} \left(\frac{\rho_0 \mp \tilde{\rho}}{\tilde{\rho}}\right)^{1/2} \exp\left\{\frac{i}{2\tilde{\zeta}}(\tilde{\rho} \mp \rho_0)^2\right\} \mu_{+} = \text{sgn}\left[\text{Im}\left(\frac{\rho_0 - \tilde{\rho}}{\sqrt{1+i\tilde{\zeta}}}\right)\right], \quad \mu_{-} = i, \quad (3.3)$$

where here and hereafter square roots are defined as $\sqrt{x} \equiv \exp\{\frac{1}{2}i \arg x\}$, $|\arg x| < \pi$ (this is the definition used in MathematicaTM, which we have used for all computations). The phases in A_{\pm} are determined by careful consideration of the steepest-descent integration contours; in A_+ , the sign switches across a Stokes line [32, 33], where the exponential is subdominant relative to the end-point contribution to be considered later. The result (3.3) reveals the reason for working with A_+ and A_- , rather than B_0 and B_1 : in this leading-order approximation, A_+ and A_- represent separate geometrical rays.

From figures 1(e)–(h), it is clear that geometrical optics captures the main features of the transition between the Hamilton–Poggendorff rings and double refraction as u increases from zero. Discrepancies between figures 1(a) and (e), and between 1(b) and (f), arise from a type of interference that we will explain later.

The new feature introduced by complexification is interference between the geometrical rays labelled + and –, even for unpolarized incident light. From (2.32), this can be significant only when $|\cos\tilde{\phi}|^2 + |\sin\tilde{\phi}|^2$ differs substantially from unity. From (2.23) and (2.24), this occurs only near the branch-points, where

$$|\cos\tilde{\phi}|^2 + |\sin\tilde{\phi}|^2 \approx \frac{2u^2}{|\tilde{\rho}^2|}. \quad (3.4)$$

(This condition appears to contradict the assumption made in expanding the Bessel functions, but we will see that it does describe the geometrical interference phenomena, and fails only in the immediate neighbourhood of the branch-points.)

Geometrical interference requires not only (3.4) but also the condition that $A_{+\text{geom}} = A_{-\text{geom}}$, implying, from (3.3), the complex condition

$$\exp\left\{-2i\rho_0\frac{\tilde{\rho}}{\tilde{\zeta}}\right\} = -i. \quad (3.5)$$

Equality of moduli now requires

$$\text{Im}\frac{\tilde{\rho}}{\tilde{\zeta}} = 0. \quad (3.6)$$

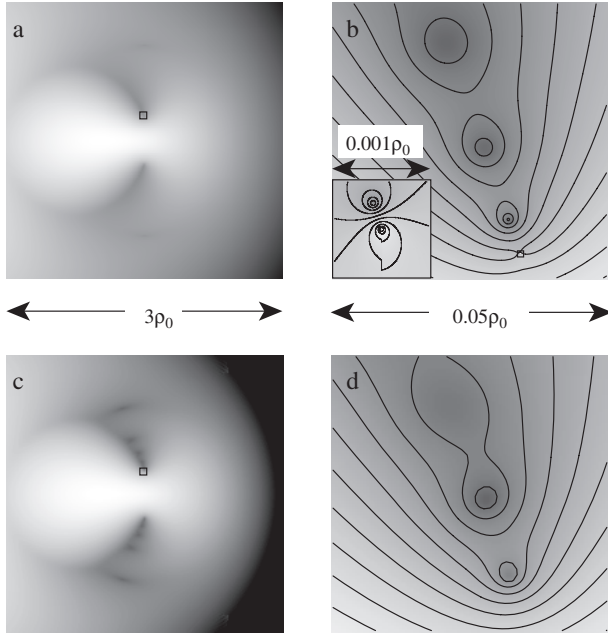


Figure 3. (a) Logarithmic density plot of geometrical intensity from figure 1(h), showing the dark ring of geometrical-optics interference described by equation (3.6). (b) $60\times$ magnification of the region indicated in (a), with contours added for clarity, showing the dark spots of complete geometrical interference given by equation (3.10); note the small bright spot at the branch-point where the geometrical intensity diverges (inset: $50\times$ magnification, also showing the dark spot nearest the branch-point and the weak unphysical discontinuity across the branch cut). (c) and (d): Logarithmic plots of the exact intensity corresponding to (a) and (b).

A short calculation shows that this restricts geometrical interference to an arc of a circle (figure 2), on which the geometrical intensity is exponentially smaller than elsewhere. The two branch-points lie on this circle, and the arc excludes the region between the branch-points. The circle is

$$(\rho - \rho_c) \cdot (\rho - \rho_c) = R_c^2, \quad (3.7)$$

where

$$\rho_c = \left\{ -\frac{u(\zeta^2 - 1)}{2\zeta}, 0 \right\}, \quad R_c = \frac{u(\zeta^2 + 1)}{2\zeta}. \quad (3.8)$$

The dark circle is clearly visible in logarithmic density plots (figures 3(a) and (c)); it is invisible in the intensity plots of figure 1.

Equality of phases in (3.5) further requires

$$\sin \left\{ 2\rho_0 \operatorname{Re} \frac{\tilde{\rho}}{\zeta} \right\} = +1 \quad (3.9)$$

giving dark spots on the dark circle, where

$$\operatorname{Re} \frac{\tilde{\rho}}{\zeta} = \frac{(n + \frac{1}{4})\pi}{\rho_0}, \quad n = \dots -1, 0, 1, \dots \quad (3.10)$$

The spots, barely visible in figures 3(a) and (c), can be seen in the magnified figures 3(b) and (d).

Receding from the branch-points, $|\cos \tilde{\phi}|^2 + |\sin \tilde{\phi}|^2$ approaches unity, and geometrical interference disappears. But

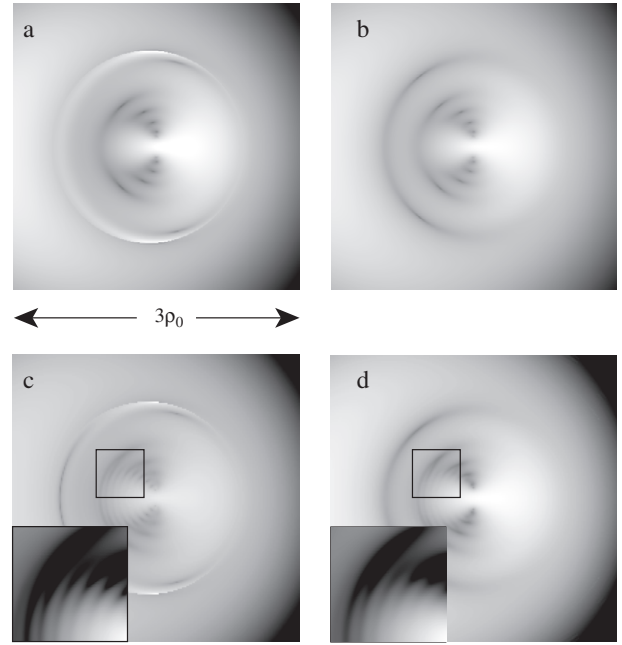


Figure 4. Logarithmic density plots of intensity corresponding to figure 1(c) with: (a) geometrical optics including the endpoint contribution from A_+ (equation (3.11)); the dark spots are the remnants of the Warnick–Arnold rings. (b) The uniform asymptotic approximation (equation (3.13)). (c) As (a), including the end-point contribution from A_- (equation (3.15)), showing additional fringes. (d) Exact intensity from the integrals (2.22).

non-geometrical interference remains, arising from the end-points $\tilde{\kappa} = 0$ of the integrals A_{\pm} . Since $\tilde{\kappa}$ is the complex length of the vector $\tilde{\kappa}$ (2.15), $\tilde{\kappa} = 0$ corresponds to the contributions from the complex degeneracies (2.11).

Consider first the interference between the contributions from the integral A_+ : a geometrical ray, and a diffracted wave scattered from the end-point $\tilde{\kappa} = 0$. This interference, which can be seen in figures 1(a) and (b), and faintly in figure 3(c), is the complexified remnant of the Warnick–Arnold rings [1, 6, 8, 9] decorating the inner Poggendorff ring of ordinary conical diffraction. It can be captured by augmenting $A_{+\text{geom}}$ with the end-point contribution

$$A_{+\text{endpoint}} = -\frac{1}{\sqrt{2\tilde{\rho}}(\rho_0 - \tilde{\rho})^{3/2}} \Theta \left(\operatorname{Re} \frac{\rho_0 - \tilde{\rho}}{\sqrt{1 + i\zeta}} \right), \quad (3.11)$$

where Θ denotes the unit step, switching on across a Stokes line, where the end-point contribution is subdominant relative to the geometrical contribution (3.3). Including $A_{+\text{endpoint}}$ does indeed capture the remnants of the Warnick–Arnold rings, as figure 4(a) clearly indicates.

But (3.11) comes at a price: a divergence on the complexified Poggendorff ring $\tilde{\rho} = \rho_0$, at

$$\xi = 0, \quad \eta = \pm\sqrt{\rho_0^2 + u^2}. \quad (3.12)$$

The divergence is visible as bright arcs near the top and bottom of figure 4(a). It can be eliminated by observing that the integrals (3.2) can be evaluated exactly, albeit somewhat impenetrably. Of several different forms [8], the one most

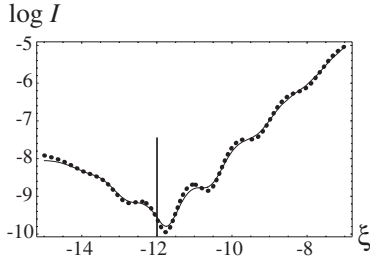


Figure 5. Intensity along the ξ axis for $\rho_0 = 20$, $\zeta = 6$, $u = 2$, showing the additional fringes visible in figures 4(c) and (d). Full curve: exact; dotted curve: geometrical approximation (3.3), augmented by the end-point contribution (3.15) from A_- . The vertical bar at $\xi = -12$ indicates the intersection of the dark geometrical circle with the ξ axis.

convenient in the complexified case is

$$A_{\pm} \approx A_{\pm \text{rings}} = \frac{2}{\sqrt{\tilde{\rho}} (1 + i\zeta)^{3/4}} f\left(\frac{(\tilde{\rho} \mp \rho_0)}{\sqrt{1 + i\zeta}}\right), \quad (3.13)$$

where f involves hypergeometric functions:

$$f(t) = \frac{1}{4\sqrt{\pi}} \left[2^{3/4} \Gamma\left(\frac{3}{4}\right) {}_1F_1\left(\frac{3}{4}, \frac{1}{2}, -\frac{1}{2}t^2\right) + 2^{-3/4} \Gamma\left(\frac{1}{4}\right) t {}_1F_1\left(\frac{5}{4}, \frac{3}{2}, -\frac{1}{2}t^2\right) \right]. \quad (3.14)$$

This powerful uniform approximation incorporates geometrical optics (including interference between complex geometrical rays) and the remanent Warnick–Arnold interferences from $\tilde{\kappa} = 0$, without diverging at the points (3.12). Figure 4(b) illustrates this.

Additional interference is associated with A_- . In the approximation (3.2), the leading-order end-point contribution to A_- vanishes in the relevant region. To determine the correct leading-order end-point contribution, (3.13) is inadequate, and it is necessary to go beyond (3.1) and include the first asymptotic corrections to J_0 and J_1 ; the result is

$$A_{-\text{endpoint}} = -\frac{1}{(2\tilde{\rho})^{3/2} \sqrt{\rho_0 - \tilde{\rho}}} \Theta\left(\text{Re} \frac{\rho_0 - \tilde{\rho}}{\sqrt{1 + i\zeta}}\right). \quad (3.15)$$

Incorporating this adds the faint additional fringes visible in figure 4(c); as figures 4(d) and 5 indicate, these are indeed present in the exact intensity.

All approximations so far described (saddle-point, uniform hypergeometric and end-point) introduce the unphysical feature that the field \mathbf{D} inherits the branch-points ρ_b (equation (2.24)) where $\tilde{\rho} = 0$. An approximation that correctly reproduces the smooth behaviour of \mathbf{D} near ρ_b is obtained by observing that for small $\tilde{\rho}$ the Bessel functions in (2.22) are slowly-varying, so that they can be approximated in terms of the $\tilde{\kappa}$ values corresponding to the stationary points of the remainder of the integrands. This leads to the complexified versions of the approximations that in the transparent case [8] describe the rings decorating the axial Raman spot in the far field,

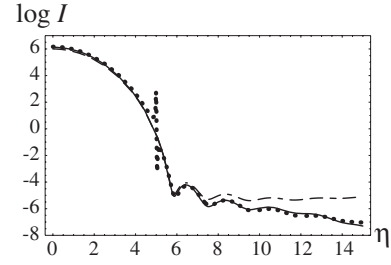


Figure 6. Intensity (2.32) along the η axis, with $\rho_0 = 20$, $\zeta = 16$, $u = 5$. Full curve: exact intensity from (2.22); dashed curve: small $\tilde{\rho}$ (Bessel) approximation (3.16); dotted curve: geometrical optics approximation (3.3), which is singular at the branch-point at $\eta = 5$.

namely

$$B_0 \approx B_{0b} = \sqrt{\frac{\pi}{2}} \frac{\rho_0}{\tilde{\zeta}^{3/2}} \exp\left\{i\left(\frac{\rho_0^2}{2\tilde{\zeta}} - \frac{1}{4}\pi\right)\right\} J_0\left(\frac{\rho_0 \tilde{\rho}}{\tilde{\zeta}}\right) \\ B_1 \approx B_{1b} = -\sqrt{\frac{\pi}{2}} \frac{\rho_0}{\tilde{\zeta}^{3/2}} \exp\left\{i\left(\frac{\rho_0^2}{2\tilde{\zeta}} + \frac{1}{4}\pi\right)\right\} J_1\left(\frac{\rho_0 \tilde{\rho}}{\tilde{\zeta}}\right). \quad (3.16)$$

Figure 6 illustrates how this approximation is regular at the branch-points and matches smoothly onto the geometrical oscillations already discussed. (In the transparent limit $u = 0$, the geometrical oscillations disappear because the polarization states are orthogonal, and (3.16) reproduces weak ‘shoulders’ [1, 8], associated with higher-than-geometrical saddle corrections.)

4. Extreme dichroism

In the previous sections, we have regarded the absorption δ as a perturbation of the biaxial birefringence described by ρ_0 . Now we briefly consider the opposite limiting case, where the crystal is refractively isotropic, so that $n_1 = n_3 = n_2$ in (1.1), and all the anisotropy is embodied in $\text{Im } \eta$. The theory is then formally identical with that for ordinary conical refraction, with the difference that the analogue of ρ_0 is imaginary, because it is proportional to the analogue of the cone half-angle A (2.2), which itself depends linearly on the differences between the components of $\text{Im } \eta$ (analogous to (2.1)). Thus

$$\rho_0 \Rightarrow i\sigma_0. \quad (4.1)$$

The components of $\text{Im } \eta$ determine a well-defined optic axis, along which the incident beam can be directed, so we can take $\kappa_0 = 0$. The light beyond the crystal is given by (2.21) with $F_0 = 0$ and $\tilde{\phi} \Rightarrow \phi$, and the integrals (2.22) with $\tilde{\rho} \Rightarrow \rho$ and (4.1). In the intensity (2.32) for unpolarized light, there is no interference term, because $|\cos \tilde{\phi}|^2 + |\sin \tilde{\phi}|^2 \Rightarrow 1$, so

$$I_{\text{unpolarized}} = |B_0|^2 + |B_1|^2 = \frac{1}{2} (|A_+|^2 + |A_-|^2). \quad (4.2)$$

Geometrical optics survives this extreme complexification, so the analogue of (3.3) is

$$A_{\pm \text{geom}} = \frac{-i}{\zeta - i} \left(\frac{\rho \mp i\sigma_0}{\rho}\right)^{1/2} \exp\left\{\frac{i}{2(\zeta - i)} (\rho \mp i\sigma_0)^2\right\}, \quad (4.3)$$

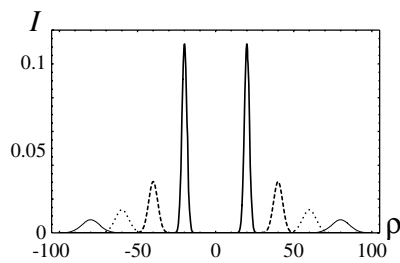


Figure 7. Extreme dichroic intensity (4.4), scaled by multiplication by $\exp(-\sigma_0^2)$, for $\sigma_0 = 10$ and $\zeta = 2$ (thick curve), 4 (dashed curve), 6 (dotted curve), 8 (thin curve). On this scale the false geometrical central singularity is invisible, and the geometrical and exact intensities are indistinguishable.

giving the intensity

$$I_{\text{unpolarized,geom}} = \frac{\sqrt{1 + \sigma_0^2/\rho^2}}{\zeta^2 + 1} \exp\left\{\frac{\sigma_0^2 - \rho^2}{\zeta^2 + 1}\right\} \cosh\left\{\frac{2\sigma_0\zeta\rho}{\zeta^2 + 1}\right\}. \quad (4.4)$$

This predicts an expanding cone of light beyond the crystal (figure 7), contrasting with ordinary conical diffraction in which there are two bright cylinders separated by the Poggendorff dark cylinder. The cone is approximately Gaussian, with radius $\sigma_0\zeta$ and width $\sqrt{1 + \zeta^2}$. In addition, the geometrical intensity possesses a weak central spike singularity, somewhat analogous to the Raman spike, but invisible in plots showing the bright cone.

Computations with the exact theory confirm these predictions, except that there is no central singularity, and not even a central maximum when ζ is large enough (for large σ_0 , there is a maximum at $\rho = 0$ when $\zeta < 1/\sqrt{3}$ and a minimum when $\zeta > 1/\sqrt{3}$).

5. Concluding remarks

There are two surprises in the theory reported here. First, the effects of dichroism and beam direction are identical if the incident beam is Gaussian. This means that the light patterns in planes beyond a dichroic crystal are not new: they were already contained (unrecognized) in the patterns of transition between conical and double refraction for a transparent crystal. Second, in the patterns themselves the geometrical intensity is decorated by several types of interference, mostly too faint to see in direct intensity plots but visible in logarithmic plots.

Each of these surprises raises a question. What happens for nonGaussian beams, for example light transmitted by a pinhole? The exact relation between beam direction and dichroism will no longer hold, but we expect a qualitative similarity. The theory is essentially the same as that in section 2, but with a Bessel function J_1 replacing the Gaussian amplitude in (2.12). This deserves further study.

Can the predicted interference fringes be observed? This would be a challenge, since the effects are faint, but they represent qualitatively new optical phenomena and so are worth searching for. Dichroism is a familiar phenomenon, but our efforts to make quantitative predictions for particular dichroic crystals were frustrated by the apparent absence of tables of the real and complex components of the dielectric

tensor in (1.1). In view of the identity between beam direction and dichroism, a more promising strategy is to study images away from the optic axes of a transparent biaxial crystal. (In the images in our experimental study (figure 2 of [9], close to the crystal, and unpublished additional images for larger values of ζ closer to that simulated in figure 1), the transition between double and conical refraction was evident, but the dynamic range was too small to show the predicted dark ring and interference fringes.)

Finally, we note a further level of generalization: incorporating optical activity (chirality) as well as dichroism. For Gaussian beams, the argument in section 2 can be easily adapted, and shows that even with chirality the effects of dichroism and beam direction are the same. In view of the rich caustic structure of chiral conical refraction for illumination along the optic axis [10], we anticipate that the transition to double refraction will be even richer than for the non-chiral case we have studied here.

Acknowledgment

Our research is supported by the Royal Society of London.

References

- [1] Berry M V and Jeffrey M R 2006 Conical diffraction: Hamilton's diabolical point at the heart of crystal optics *Prog. Opt.* at press
- [2] Lunney J G and Weaire D 2006 *Europhys. News* **37** 26–9
- [3] O'Hara J G 1982 The prediction and discovery of conical refraction by William Rowan Hamilton and Humphrey Lloyd (1832–1833) *Proc. R. Ir. Acad. A* **82** 231–57
- [4] Hamilton W R 1837 Third supplement to an essay on the theory of systems of rays *Trans. R. Ir. Acad.* **17** 1–144
- [5] Belskii A M and Khapalyuk A P 1978 Internal conical refraction of bounded light beams in biaxial crystals *Opt. Spectrosc. (USSR)* **44** 436–9
- [6] Warnick K F and Arnold D V 1997 Secondary dark rings of internal conical refraction *Phys. Rev. E* **55** 6092–6
- [7] Berry M V, Jeffrey M R and Mansuripur M 2005 Orbital and spin angular momentum in conical diffraction *J. Opt. A: Pure Appl. Opt.* **7** 685–90
- [8] Berry M V 2004 Conical diffraction asymptotics: fine structure of Poggendorff rings and axial spike *J. Opt. A: Pure Appl. Opt.* **6** 289–300
- [9] Berry M V, Jeffrey M R and Lunney J G 2006 Conical diffraction: observations and theory *Proc. R. Soc. A* **462** 1629–42
- [10] Berry M V and Jeffrey M R 2006 Chiral conical diffraction *J. Opt. A: Pure Appl. Opt.* **8** 363–72
- [11] Belsky A M and Stepanov M A 2002 Internal conical refraction of light beams in biaxial gyrotropic crystals *Opt. Commun.* **204** 1–6
- [12] Indik R A and Newell A C 2006 Conical refraction and nonlinearity *Opt. Express* **14** at press
- [13] Landau L D, Lifshitz E M and Pitaevskii L P 1984 *Electrodynamics of Continuous Media* (Oxford: Pergamon)
- [14] Born M and Wolf E 2005 *Principles of Optics* (London: Pergamon)
- [15] Berry M V 2004 Physics of nonhermitian degeneracies *Czech. J. Phys.* **54** 1040–7
- [16] Voigt W 1902 On the behaviour of pleochroitic crystals along directions in the neighbourhood of an optic axis *Phil. Mag.* **4** 90–7
- [17] Ramachandran G N and Ramaseshan S 1961 *Crystal Optics in Handbuch der Physik* vol XXV/I, ed H Flügge (Berlin: Springer)

- [18] Pancharatnam S 1955 The propagation of light in absorbing biaxial crystals—I. Theoretical *Proc. Indian Acad. Sci.* **42** 86–109
- [19] Pancharatnam S 1955 The propagation of light in absorbing biaxial crystals—II. Experimental *Proc. Indian Acad. Sci.* **42** 235–48
- [20] Berry M V and Dennis M R 2003 The optical singularities of birefringent dichroic chiral crystals *Proc. R. Soc. A* **459** 1261–92
- [21] Dreger M A 1999 Optical beam propagation in biaxial crystals *J. Opt. A: Pure Appl. Opt.* **1** 601–16
- [22] Lloyd H 1837 On the phenomena presented by light in its passage along the axes of biaxial crystals *Trans. R. Ir. Acad.* **17** 145–58
- [23] Potter R 1841 An examination of the phaenomena of conical refraction in biaxial crystals *Phil. Mag.* **8** 343–53
- [24] Raman C V, Rajagopalan V S and Nedungadi T M K 1941 Conical refraction in naphthalene crystals *Proc. Indian Acad. Sci. A* **14** 221–7
- [25] Schell A J and Bloembergen N 1978 Laser studies of internal conical diffraction. I. Quantitative comparison of experimental and theoretical conical intensity distribution in aragonite *J. Opt. Soc. Am.* **68** 1093–8
- [26] Mikhailychenko Y P 2005 Large scale demonstrations on conical refraction, <http://www.demophys.tsu.ru/Original/Hamilton/Hamilton.html>
- [27] Fève J P, Boulanger B and Marnier G 1994 Experimental study of internal and external conical refraction in KTP *Opt. Commun.* **105** 243–52
- [28] Deschamps G A 1971 Gaussian beam as a bundle of complex rays *Electron. Lett.* **7** 684–5
- [29] Poggendorff J C 1839 Ueber die konische refraction *Pogg. Ann.* **48** 461–2
- [30] Heiss W D and Harney H L 2001 The chirality of exceptional points *Eur. Phys. J. D* **17** 149–51
- [31] Abramowitz M and Stegun I A 1972 *Handbook of Mathematical Functions* (Washington: National Bureau of Standards)
- [32] Berry M V 1989 Stokes' phenomenon; smoothing a Victorian discontinuity *Publ. Math. Institut des Hautes Etudes Sci.* **68** 211–21
- [33] Berry M V 1989 Uniform asymptotic smoothing of Stokes's discontinuities *Proc. R. Soc. Lond. A* **422** 7–21